



Brain Strain from Motion of Sparse Markers

Zhou Zhou, Xiaogai Li, Svein Kleiven

Neuronic Engineering, KTH Royal Institute of Technology, Stockholm, Sweden

Warren N. Hardy

Virginia Tech-Wake Forest Center for Injury Biomechanics, Blacksburg, Virginia, USA

ABSTRACT – Brain strain secondary to head impact or inertial loading is closely associated with pathologic observations in the brain. The only experimental brain strain dataset under loadings close to traumatic levels was calculated by imposing the experimentally measured motion of markers embedded in the brain to an auxiliary model formed by triad elements (Hardy et al., 2007). However, fidelity of the calculated strain as well as the suitability of using triad elements for three-dimensional (3D) strain estimation remains to be verified. Therefore, this study proposes to use tetrahedron elements as a new approach to estimate the brain strain. Fidelity of this newly-proposed approach along with the previous triad-based approach is evaluated with the aid of three independently-developed finite element (FE) head models by numerically replicating the experimental impacts and strain estimation procedures. Strain in the preselected brain elements obtained from the whole head simulation exhibits good correlation with its tetra estimation and exceeds its triad estimation, indicating that the tetra approach more accurately estimates the strain in the preselected region. The newly calculated brain strain curves using tetra elements provide better approximations for the 3D experimental brain deformation and can be used for strain validation of FE models of human head.

KEYWORDS – Traumatic brain injury; brain strain; motion of markers; strain estimation; finite element head model

INTRODUCTION

Traumatic brain injury (TBI) is a substantial public health threat worldwide with an estimated number of TBI victims over 10 million each year (Hyder et al., 2007). Although a complete understanding of the relationship between mechanical input and brain injury remains to be further elaborated, it has been hypothesized that brain strain might be correlated with the physiologic damage in TBI victims (Fahlstedt et al., 2015, Gennarelli et al., 1989, Kleiven, 2007, Zhou et al., 2019). Thus, accurate measurement of brain deformation secondary to head impact or inertial loading may help in estimating brain injury and forms a foundation for designing protective devices and therapeutic strategies.

Though it has already been theoretically established for decades that deformation can be estimated from the displacement field, details of brain deformation remain largely elusive, especially in the traumatic

scenarios. Two subsequent physical-model studies (Margulies et al., 1990, Meaney et al., 1995) adopted high-speed movie camera to film the motion of an orthogonal grid embedded within gel-filled animal and human skulls. The shear strain was defined as the angle variation of the grid within its embedded plane. The maximum shear strain was reported to be 0.05-0.22 under pure coronal accelerations at levels associated with concussion or diffuse axonal injury. Later, Hardy et al. (2007) used bi-plane high-speed X-ray to track the motion of neutral density targets (NDTs) implanted in cluster array within the post-mortem human surrogate (PMHS) heads secondary to various impact modes. Deformation within the volume occupied by the implanted NDT clusters was estimated by an auxiliary model with triad elements. Since the experimentally measured NDT motions along three directions were used to excite the auxiliary model, three-dimensional (3D) brain strain was obtained. The peak maximum principal and maximum shear strains were reported with magnitudes about 0.03-0.09 (Zhou et al., 2018).

Brain deformation has also been estimated in the living human brain, though the test conditions are far

Address correspondence to Zhou Zhou, Neuronic Engineering, KTH Royal Institute of Technology, Stockholm, Sweden. Electronic mail: zhous@kth.se

from injury levels. Bayly et al. (2005) implemented tagged magnetic resonance imaging (MRI) technique, in which tagged lines were inscribed to the imaging sequences, to identify the brain motion under voluntary test. Due to the slow image acquisition rate, the strain was estimated by evaluating different time points from manually repeated trials. Given that the out-of-plane motion, i.e. motion perpendicular to the loading plane, was minimal, the two-dimensional (2D) planar strain was reported with a magnitude about 0.02-0.05. This tagged MRI approach was subsequently implemented to other voluntary scenarios with the 2D planar strain consistently being reported (Feng et al., 2010, Knutson et al., 2014, Sabet et al., 2008). A recent study by Gomez et al. (2018) extended the in-vivo brain strain measurement into 3D by integrating the harmonic phase analysis of tagged MRI with finite element (FE) approach.

In addition, FE head models offer detailed spatiotemporal strain information (Ho et al., 2017, Kleiven, 2007, Mao et al., 2013, Zhou et al., 2019). The accuracy of the numerically-predicted strain requires at least that the FE head model has been extensively validated against experimental strain data. Since such an experimental brain strain dataset is lacking, computational prediction of the brain deformation remains uncertain (Bayly et al., 2012, Giordano and Kleiven, 2016).

For all the existing brain strain estimation efforts, the one by Hardy et al. (2007) is particularly illuminating since it provided 3D brain deformation of human specimens under impacts that might result in trauma. Previous studies have shown that fidelity of the strain deduced from the motions of a finite number of markers, such as the case in Hardy et al. (2007), depended not only on the nature of actual deformation field but also on the estimation approach (Kindberg et al., 2007, Průša et al., 2013). Considering the 3D nature of the brain displacement field in Hardy et al. (2007), it is hypothesized that an approach using solid elements, instead of triad elements, provides a better approximation for the 3D experimental strain.

Thus, the purpose of the current study is to propose a new approach, in which tetrahedron elements are adopted, to estimate the brain strain in Hardy et al. (2007). The fidelity of this newly proposed tetra approach along with the previously adopted triad approach is evaluated with the aid of FE head models by numerically replicating the experimental impacts and strain estimation procedures. By comparing the

strain in certain preselected regions as well as its estimates, superiority of the tetra approach in terms of providing a better approximation for the 3D deformation field is revealed.

METHODS

Experimental brain strain estimation

The brain is expected to undergo large deformation secondary to loadings as in Hardy et al. (2007). Ideally, the brain deformation can be accurately determined (referred to as true experimental strain) by analyzing motion of embedded markers, when the spatial and temporal resolution of the marker motion measurement is guaranteed (Bayly et al., 2012). Practically, Hardy et al. (2007) implanted 7 NDTs in cluster array with the center target being 10 mm from the other six targets. Strain in the brain volume encompassed by the NDT cluster was calculated by imposing the experimentally measured NDT motions to an auxiliary model that was developed by connecting each NDT to its neighboring counterparts to form triad elements (Figure 1 (b)) (Hardy et al., 2007, Zhou et al., 2018). Thus, these triad elements had 2D descriptions in the local element coordinate systems although being 3D in terms of degrees of freedom. This strain calculation approach is hereafter referred to as the triad approach.

However, as stated by Waldman et al. (1985), experimental strain might not be well represented when planar elements were used for 3D strain estimation. Thus, based on the NDT deploying characteristics in Hardy et al. (2007), tetrahedron elements are adopted to alternatively estimate the experimental brain strain. For a typical cluster with all 7 associated NDTs being tracked successfully, 8 tetrahedron elements can be developed by connecting each NDT to its neighboring counterparts (Figure 1(c)). Identical to the triad approach, the tracked motions are used to excite the tetrahedron model and the strain results of all available tetrahedron elements are averaged to provide a general response within the region of each cluster. This newly proposed approach is referred to as the tetra approach.

Of both approaches, the first principal Green-Lagrangian strain (referred to as principal strain) and the maximum shear Green-Lagrangian strain (referred to as shear strain) are extracted. Since 3D displacements are prescribed to all FE nodes in both the triad and tetra approaches, resultant strain responses are independent of the modeling choices, such as element formulation, material properties, etc.

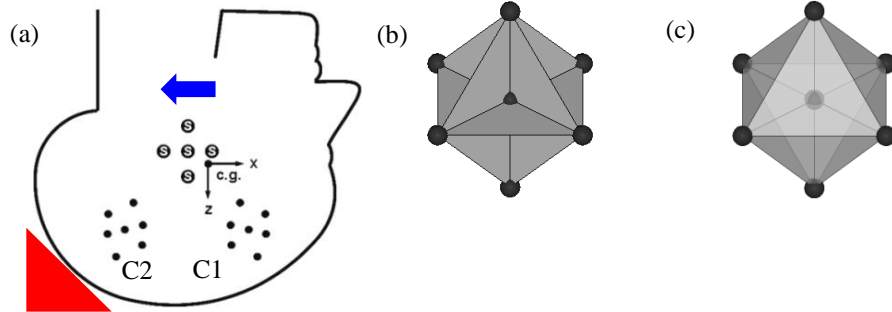


Figure 1. (a) Representative sketch of NDT cluster implanting schemes. For a given head, two NDT clusters were implanted as cluster 1 (C1) and cluster 2 (C2). (b) Strain estimation by the triad approach with NDT as black spheres while triad elements in grey and mesh line in black. (c) Strain estimation by the tetra approach with NDT as black spheres while tetrahedron elements in grey and mesh line in black. To visualize the center NDT, all tetrahedron elements are shown in translucency.

Fidelity evaluation of strain estimation approach

Comparing to the idealized situation that the deformation gradient is ascertained by analyzing motion of the markers with guaranteed spatial and temporal resolution, current brain strain estimation based on the motion of 7 NDTs, both for the triad approach and for the tetra approach, confronts the limitation of reduced marker resolution. Hypothetically, fidelity of these two approaches can be evaluated by comparing the estimated experimental strain against the true experimental strain. Unfortunately, the true experimental strain remains unknown. Thus, it is impossible to assess the strain estimation approach from the experimental respect.

To overcome the infeasibility of using the true experimental strain to assess the fidelity of these two strain estimation approaches, the Kungliga Tekniska Högskolan (KTH) detailed head model (Figure 2 and Appendix A), as a surrogate for the cadaver head, is alternatively employed to replicate experimental impacts and strain estimation approaches. 6 representative experiments are selected, including C288-T3 for sagittal impact, C380-T2 for horizontal impact, C380-T1, C380-T3, C380-T4 and C380-T6 for coronal impact. Given its completeness in motion measurement, cluster 1 (C1) is selected as the cluster of interest. The rationale of evaluating the fidelity of strain estimation approaches with the aid of an FE head model is explained in Figure 3 using C288-T3 as an example. By imposing the experimental loading to the FE head model, the numerical brain deformation field can be obtained by analyzing the displacement of the nodes, which can be regarded as numerical substitutes for the NDTs. The aiding FE model exhibits an average element size of 0.6 mm. The node nearest to the initial position of the

experimental NDT target is taken as the NDT representation in the model. The spatial deviation between the experimental NDTs and identified representative nodes is less than 0.35 mm. These identified nodes are further used to select the brain elements representing the tissue encompassed by the NDT cluster. For a typical NDT cluster occupying tissue volume about 1 ml, about 600 elements are selected (Figure 3 (b)). The strain of all selected brain elements are directly extracted from the whole head model simulation and then averaged. To replicate the experimental strain estimation procedures, the identified nodes are used to establish one model with triad elements (Figure 3 (c)) and one model with tetrahedron elements (Figure 3 (d)), respectively. Nodal motion responses obtained from the whole head model simulation are used to drive the models and the strains of all affiliating elements are averaged.

It should be clarified that the strain in the preselected brain elements obtained from the whole head simulation should be seen as a numerical substitute for the true experimental strain. The strains estimated by the triad approach and the tetra approach with the numerically predicted nodal motion as excitation are the substitutes for the experimental strains estimated by the same approaches with the experimentally measured NDT motion as excitation. When evaluating the fidelity of these two strain estimation approaches, strain in the representative brain elements from the whole head simulation serves as the reference. Fidelity of these two strain estimation approaches is evaluated by comparing the reference with its triad and tetra estimations, respectively. For these two approaches, the one with superior fidelity revealed with the aid of the FE head model should be used to estimate the experimental brain strain in Hardy et al. (2007).

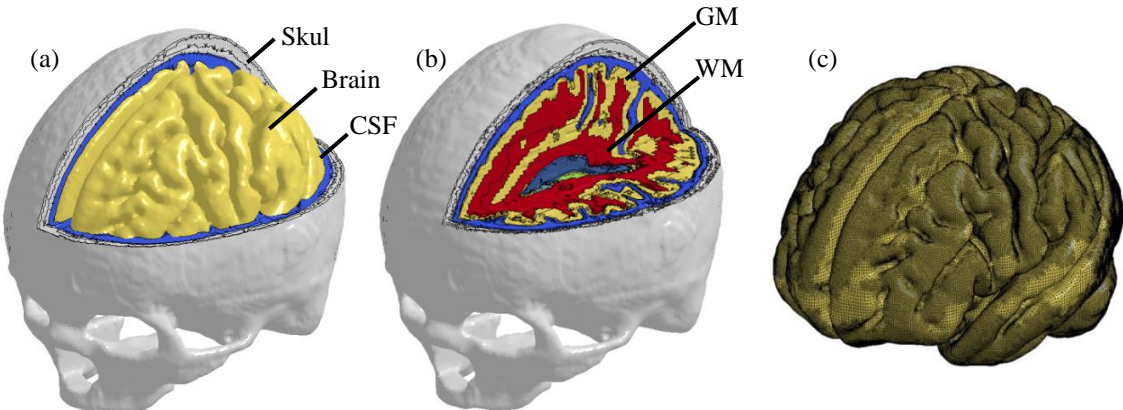


Figure 2. Isometric views of the FE human head model. (a) Head model with the brain and cerebrospinal fluid (CSF) exposed. (b) Head model with the gray matter (GM) and white matter (WM) exposed. (c) Brain model with visible mesh.

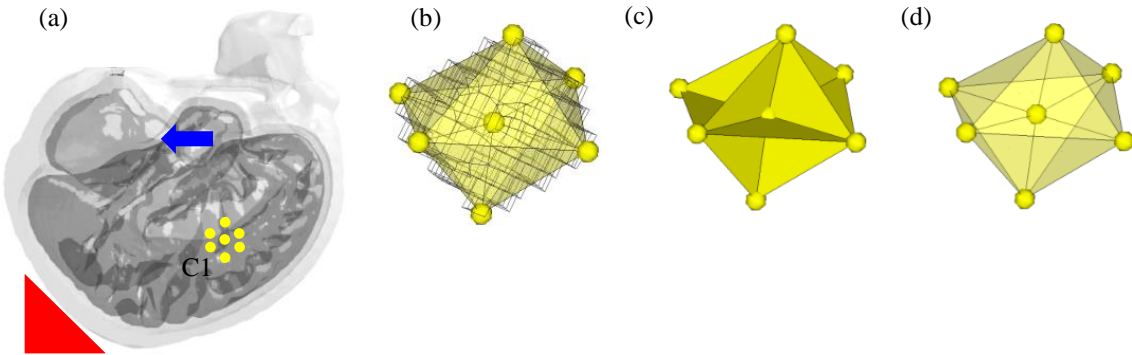


Figure 3. Numerical replication of C288-T3 and strain estimation procedures. (a) Sketch of head impact simulation of C288T3 with the NDT representative nodes for C1 as yellow dots. (b) Selected brain elements representing the brain tissue encompassed by C1. For better illustration, the model in the tetra approach is superimposed on the representative brain elements shown as wireframe with black mesh line. (c) Strain estimation by the triad approach with the NDT representative nodes as yellow spheres, triad elements in yellow, and mesh line in black. (d) Strain estimation by the tetra approach with the NDT representative nodes as yellow spheres, tetrahedron elements in yellow, and mesh line in black. To visualize the center NDT representative node, all tetrahedron elements are shown in translucency.

RESULTS

Estimated experimental brain strain

Following the selection criteria established by Zhou et al. (2018), 15 NDT clusters from 14 impacts with all 7 associated NDTs being measured successfully are chosen for strain calculation, using both the triad and tetra approaches (Figure 4). It is noted that, for all involved clusters, strain estimated by the tetra

approach is consistently larger than its counterpart by the triad approach. The peak principal strain falls within the range of 0.072 to 0.220 for the tetra approach, and 0.035 to 0.094 for the triad approach. For the shear strain, the peaks vary from 0.082 to 0.160 for the tetra approach, and 0.039 to 0.091 for the triad approach. An additional model is developed in Appendix B to derive the strain in cluster in which six NDTs were reliably tracked.

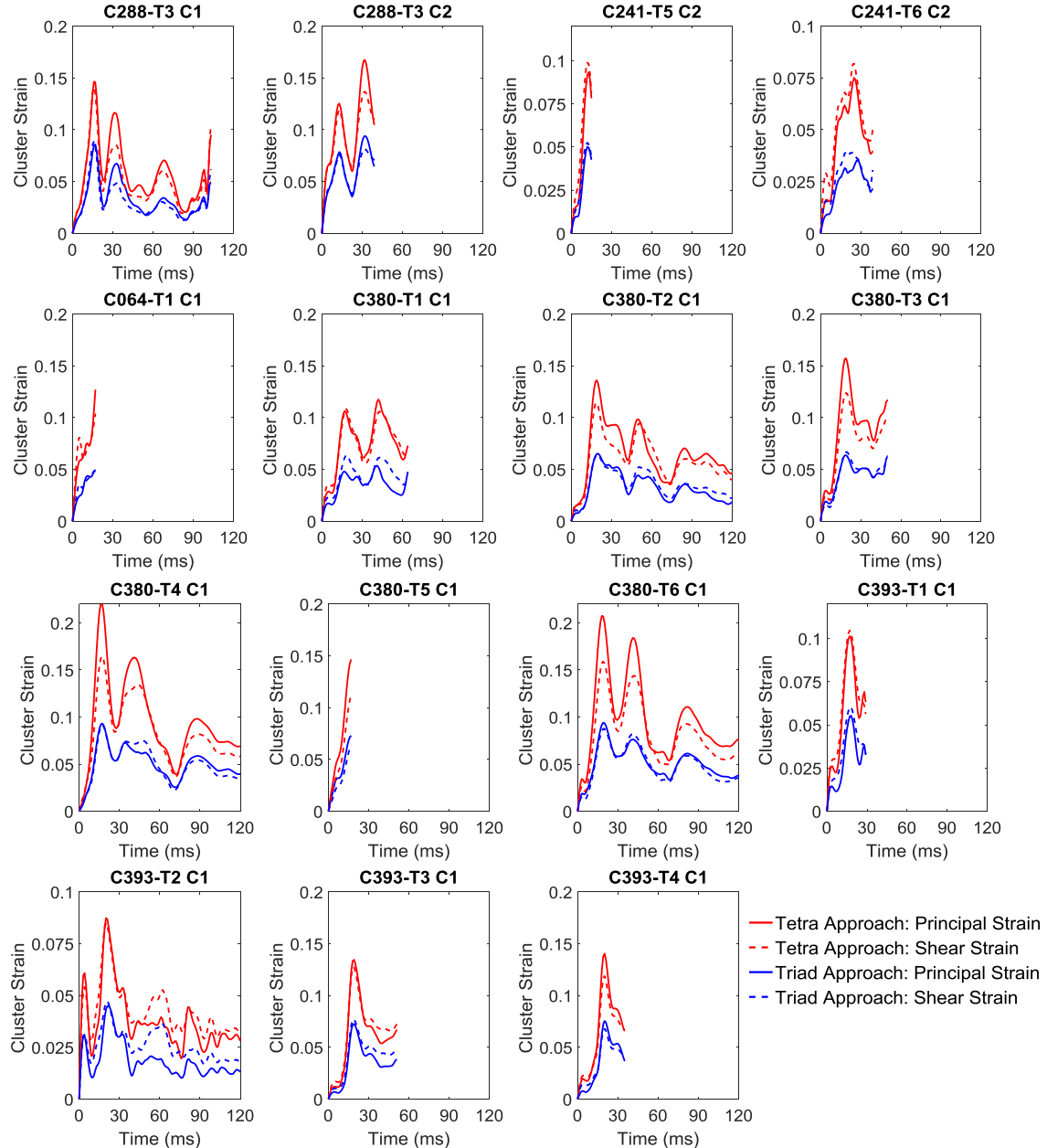


Figure 4. Comparisons of strain responses of 15 NDT clusters estimated by the triad approach and the tetra approach.

Strain estimation approach evaluation

The principal strain is employed as a representative index to delineate the numerical evaluation results regarding the fidelity of these two strain estimation approaches (Figure 5). For all the six clusters, strain in the representative brain elements obtained from the

whole head simulation, serving as the reference, exhibits good correlation with its tetra estimation with peak differences less than 0.01, and exceeds its triad estimation with peak difference around 0.03 on average. Such results indicate that the tetra approach provides a better approximation for the strain in the representative brain elements.

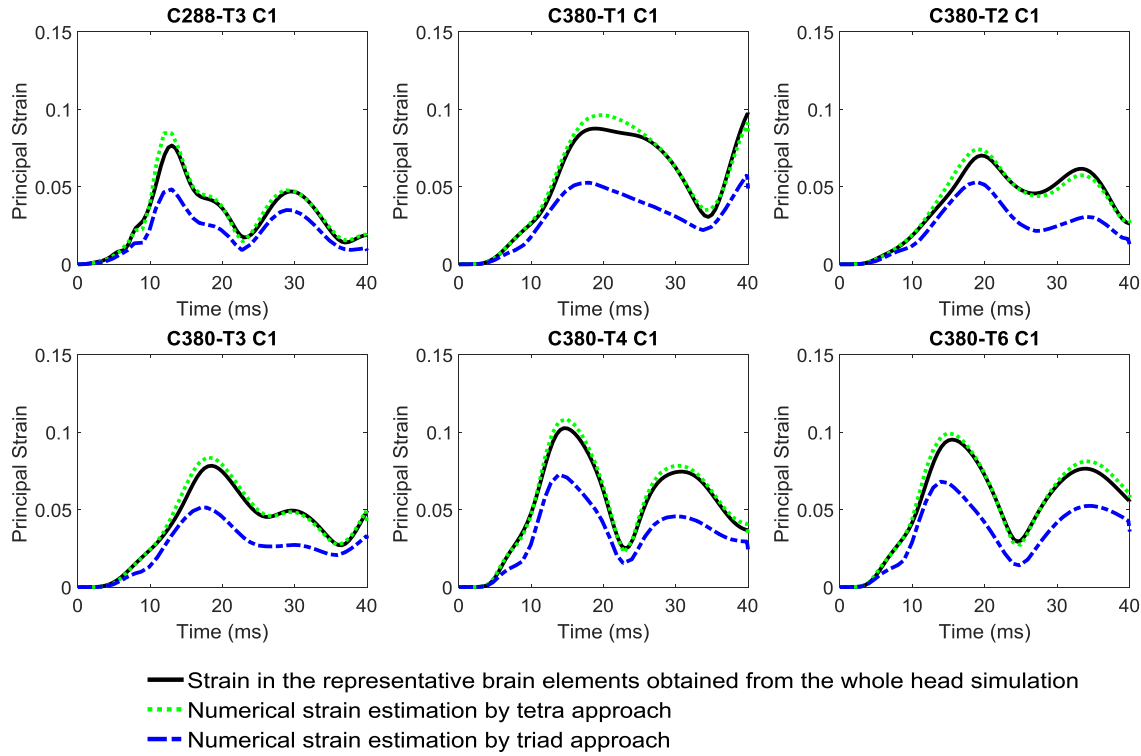


Figure 5. Numerical comparison of strain in the representative brain elements obtained from the whole head simulation and its estimations by the tetra approach and the triad approach.

DISCUSSION

The current study proposes a new approach to estimate experimental brain strain from motion of sparse markers. The fidelity of this newly implemented tetra approach along with the previously adopted triad approach is evaluated with the aid of the KTH detailed head model by replicating the experimental impacts and strain estimation procedures. It is revealed that the strain in the preselected brain elements obtained from the whole head simulations exhibits good correlation with its tetra estimation and exceeds its triad estimation, suggesting that the tetra approach contributes to a better approximation for the strain in the preselected region. These results verify that the tetra approach should be adopted to estimate the experimental brain strain in Hardy et al. (2007). The newly calculated strain curves by tetra elements can be used to validate the strain response of FE models of human head.

Current advocacy of the tetra approach for the brain motion analysis agrees with the 3D strain estimation strategies in the other biological tissues. Waldman et al. (1985) used high-speed simultaneous biplane cineradiography to record the motion of lead beads

implanted in closely-spaced column arrays at a single site on the left ventricular wall of mongrel dogs. Tetrahedral elements forming any four non-coplanar markers were used to analyze the bead motion with components parallel and perpendicular to the epicardium. Kolaczek et al. (2016) tracked motion of implanted markers in the meniscus under the loaded and unloaded human cadaveric knee joint. The strain was calculated by imposing the tracked motion to a tetrahedral element developed by connecting four non-coplanar markers. This approach was subsequently employed to compare the strain responses in native medial menisci and in allograft-transplanted medial menisci (Kolaczek et al., 2019). The prevalence of using the tetra approach for 3D strain estimation increases the credence of current advocacy. Moreover, the current study proposes a strain estimation framework with guaranteed fidelity that can be used for future experimental strain calculation.

A comparison of strain peaks estimated by the triad and tetra approaches to earlier studies is presented in Table 1. The tetra-estimated strain peaks agree well with the strain magnitudes measured from physical models (Margulies et al., 1990, Meaney et al., 1995) secondary to pure rotations close to the loading

severities in Hardy et al. (2007). The triad-estimated strain peaks largely overlap with the maximum strain peaks from volunteer tests whose loading conditions were far from injury levels, indicating the triad approach underestimates the experimental brain strain magnitude. Such underestimations by the triad approach are also noted in previous cardiovascular studies. Fenton et al. (1978) and Waldman et al. (1985) calculated the transmural myocardial strain by analyzing the motion of lead markers implanted in the ventricular wall, with the aid of planar elements and tetrahedron elements, respectively. It was reported that the tetra-estimated cardiovascular strain was larger than its counterpart estimated by planar elements (Waldman et al., 1985).

The tetra-estimated strain exhibits a peak of 0.07-0.22 for the principal component and 0.08-0.16 for the shear component, falling within the range of existing brain injury thresholds associated with strain. Thibault et al. (1990) performed uniaxial stretch experiments on isolated giant squid axon and found a maximal principal strain around 0.10 to cause reversible injury to the axons, which could be used as a conservative threshold for concussion. By detecting the functional impairment of the optic nerve of guinea pig secondary to a controlled displacement, Bain and Meaney (2000) estimated an optimal axial strain threshold for electrophysiological impairment to be 0.18. An in vitro study by Morrison et al. (2003) noted that strain level over 0.20 led to significant cell death in the cultured hippocampus

slice. The general approximation of the current tetra-estimated strain magnitude to the previously established strain thresholds indicates that some of the loadings in Hardy et al. (2007) may reach the level causing physiologic injury.

Following the previous effort in Zhou et al. (2018) in which the triad-estimated strain was presented, the Pearson correlation coefficient is determined to assess the correlation between the tetra-estimated strain peaks and the average cluster brain-skull relative motion peaks of all 15 NDT clusters. The correlation is considered significant for $p < 0.01$. As plotted in Figure 6, no significant correlations are observed between the experimentally measured brain-skull relative motion peaks and tetra-estimated brain strain peaks, neither for the principal strain nor for the shear strain. Such lacking of correlation appears to support our previous recommendation that an FE head model with intended use for strain prediction should be validated against experimental brain deformation data, and not just the brain-skull relative motion as is the typical practice. This recommendation is also supported by Zou et al. (2007), who reported that brain-skull relative motion could be further decomposed into a rigid-body displacement component and a deformation component. Considering that the strain is exclusively determined by the deformation component, a direct evaluation of brain strain response can enhance the confidence of using FE head models for strain-based TBI prediction.

Table 1. Comparison of peak brain strain from available studies.

Approach	Study	Acceleration/Velocity range	Peak strain
Physical model	Margulies et al. (1990)	Angular acceleration: 3700-69600 rad/s ²	Shear strain: 0.07-0.22
	Meaney et al. (1995)	Angular acceleration: 5000-200000 rad/s ²	Shear strain: 0.05-0.17
Volunteer test	Bayly et al. (2005)	Linear acceleration: 2-3 g	Principal strain: 0.02-0.05
	Sabet et al. (2008)	Angular acceleration: 250-300 rad/s ²	Principal strain: 0.06
	Feng et al. (2010)	Linear acceleration: 1.5 g Angular acceleration: 120-140 rad/s ²	Principal strain: 0.05-0.07
PMHS test	Triad approach (Zhou et al., 2018)	Linear acceleration: 38-291 g Angular acceleration: 2370-24206 rad/s ²	Principal strain: 0.035-0.094 Shear strain: 0.039-0.091
	Tetra approach (Current study)	Angular velocity: 20.3 ± 5.7 rad/s	Principal strain: 0.07-0.22 Shear strain: 0.08-0.16

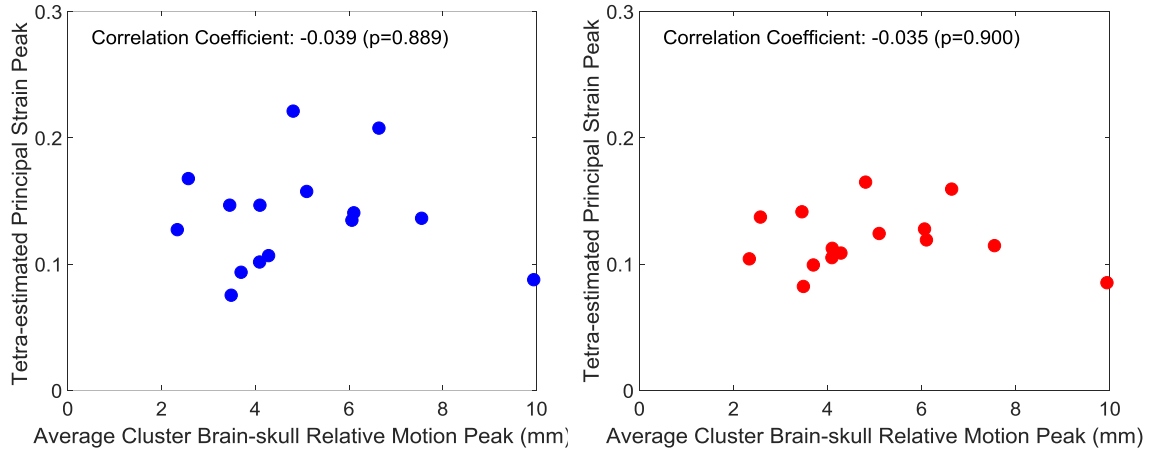


Figure 6. Scatter plot showing average cluster brain-skull relative motion peaks and tetra-estimated strain peaks and Pearson correlation results (left: principal strain; right: shear strain).

A high-resolution FE head model, as a surrogate for the cadaver head, is used to simulate the experimental impacts and to perform the strain estimation procedures in the current study. The strain in the preselected brain elements obtained from the whole head simulations is a numerical substitute for the true experimental strain. The strains estimated by the triad approach and the tetra approach with the excitation as the numerically predicted nodal motion are the substitutes for the experimental strains estimated by the same approaches with the excitation as the experimentally measured NDT motion. Thus, when evaluating the fidelity of these two strain estimation approaches using the numerical model, strain in the representative brain elements from the whole head simulation serves as the reference. It is found that the strain in the preselected brain elements obtained from the whole head simulations correlates well with its tetra estimation. Thus, it is extrapolated that the tetra approach should be used to calculate the strain in Hardy et al. (2007), providing a better approximation for the true experimental strain.

The accuracy of computationally predicted brain strain depends heavily on the modeling strategy of the FE model. For a given head model, the predicted strain magnitude is heavily depended on the material modeling of the brain. As detailed in Appendix C, to test the dependency of the evaluation results regarding the fidelity of strain estimation approach on the brain stiffness and the constitutive law used for the brain, three additional models are developed by

modifying the brain material modeling in the KTH detailed head model. To further test the model-dependency of the evaluation results, two independently-developed head models, i.e. the Total Human Model for Safety (THUMS) head model (Kimpara et al., 2006) and the Global Human Body Models Consortium (GHBMC) head model (Mao et al., 2013), are selected. These five models are employed to simulate one representative experimental impact (C380-T4) as well as the associated strain estimation procedures. It can be noted that, for all the five models, strains in the preselected brain elements from the whole head simulation correlate well with their tetra estimations (Figure 7), implying that the evaluation results regarding the fidelity of strain estimation approach are independent of not only the brain modelling strategy in a given head model, but also the head model employed. Such results further reinforce the advocacy that the tetra approach should be used to estimate the experimental brain strain in Hardy et al. (2007).

As partially revealed in Figure 7 and Figure C6, the evaluation results regarding the fidelity of strain estimation approach is independent of the strain validation performance of the head model. It is believed any head model with sufficient resolution to resolve the cluster geometry could be used for this evaluation, since only the strain extraction approach is evaluated using the head models.

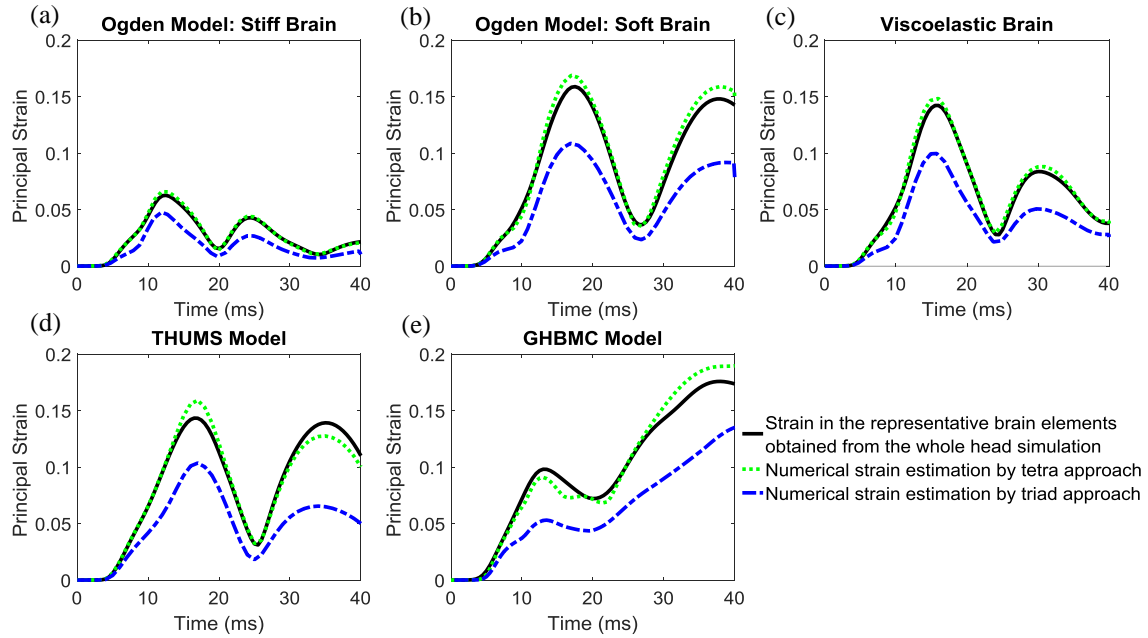


Figure 7. Numerical comparison of strain in the representative brain elements obtained from the whole head simulation and its estimations by the tetra approach and the triad approach for the C1 in experiment C380-T4. (a) Strain results of the KTH detailed head model with brain represented by an Ogden-based material with “stiff” constants. (b) Strain results of the KTH detailed head model with brain represented by an Ogden-based material with “soft” constants. (c) Strain results of the KTH detailed head model with brain represented by a viscoelastic material. (d) Strain results of the THUMS head model. (e) Strain results of the GHBMC head model.

For all the models used in the current study, it is found that the strain in the preselected brain elements obtained from the whole head simulation correlates well with its tetra estimation. However, such a finding cannot be extended to the other models with coarse meshes that suffer deficiency in NDT location representation. Thus, when the future modeler attempts to use the newly calculated strain curves by tetra elements to validate the strain response of a head model, the tetra approach is suggested to be used to extract strain from the whole head model simulation. Only under the condition that, for a given region in the head model representing the NDT-occupied volume, strain from the whole head simulation agrees well its tetra counterpart, both approaches can be used. In addition, the spatial accuracy of experimental NDT location representation in the FE model is suggested to be reported, which were commonly missing in previous publications about model validation using the data from Hardy et al. (2001) and/or Hardy et al. (2007).

A discussion regarding limitations is available in Hardy et al. (2007) for the experiments and in Kleiven and Hardy (2002) for the numerical replications.

CONCLUSION

The current study proposes a tetra approach to estimate the experimental brain strain. The fidelity of this tetra approach as well as the previously adopted triad approach is assessed with the aid of three independently-developed FE head models by replicating the experimental impacts and strain estimation procedures. The good correlation between the strain in preselected brain elements obtained from the whole head simulation and its tetra estimation indicates that the tetra approach provides a better approximation for the 3D experimental brain deformation. The newly calculated strain curves by tetra elements can be used to validate the strain response of FE models of human head.

ACKNOWLEDGMENTS

This research has received funding from the European Union’s Horizon 2020 research and innovation programme under the Marie-Curie grant agreement No. 642662 and from the BioMEx center at KTH. The simulations were performed on resources provided by the Swedish National Infrastructure for Computing (SNIC) at the PDC center.

REFERENCES

- Aimedieu, P., and Grebe, R. (2004) Tensile strength of cranial pia mater: preliminary results. *Journal of Neurosurgery* 100 (1): 111-114.
- Bain, A.C., and Meaney, D.F. (2000) Tissue-level thresholds for axonal damage in an experimental model of central nervous system white matter injury. *Journal of Biomechanical Engineering* 122 (6): 615-622.
- Bayly, P., Cohen, T., Leister, E., Ajo, D., Leuthardt, E., and Genin, G. (2005) Deformation of the human brain induced by mild acceleration. *Journal of Neurotrauma* 22 (8): 845-856.
- Bayly, P.V., Clayton, E.H., and Genin, G.M. (2012) Quantitative imaging methods for the development and validation of brain biomechanics models. *Annual Review of Biomedical Engineering* 14: 369-396.
- Fahlstedt, M., Depreitere, B., Halldin, P., Vander Sloten, J., and Kleiven, S. (2015) Correlation between injury pattern and finite element analysis in biomechanical reconstructions of traumatic brain injuries. *Journal of Biomechanics* 48 (7): 1331-1335.
- Feng, Y., Abney, T.M., Okamoto, R.J., Pless, R.B., Genin, G.M., and Bayly, P.V. (2010) Relative brain displacement and deformation during constrained mild frontal head impact. *Journal of the Royal Society Interface* 7 (53): 1677-1688.
- Fenton, T., Cherry, J., and Klassen, G. (1978) Transmural myocardial deformation in the canine left ventricular wall. *American Journal of Physiology-Heart and Circulatory Physiology* 235 (5): H523-H530.
- Gennarelli, T., Thibault, L., Tipperman, R., Tomei, G., Sergot, R., Brown, M., Maxwell, W., Graham, D., Adams, J., and Irvine, A. (1989) Axonal injury in the optic nerve: a model simulating diffuse axonal injury in the brain. *Journal of Neurosurgery* 71 (2): 244-253.
- Giordano, C., and Kleiven, S. (2016) Development of an unbiased validation protocol to assess the biofidelity of finite element head models used in prediction of traumatic brain injury. *Stapp Car Crash Journal* 60: 363-471.
- Gomez, A.D., Knutsen, A., Xing, F., Chan, D., Lu, Y.-C., Pham, D., Bayly, P.V., and Prince, J.L. (2018) 3D Measurements of Acceleration-Induced Brain Deformation via Harmonic Phase Analysis and Finite-Element Models. *IEEE Transactions on Biomedical Engineering*.
- Hardy, W.N., Foster, C.D., Mason, M.J., Yang, K.H., King, A.I., and Tashman, S. (2001) Investigation of head injury mechanisms using neutral density technology and high-speed biplanar X-ray. *Stapp Car Crash Journal* 45: 337-368.
- Hardy, W.N., Mason, M.J., Foster, C.D., Shah, C.S., Kopacz, J.M., Yang, K.H., King, A.I., Bishop, J., Bey, M., and Anderst, W. (2007) A study of the response of the human cadaver head to impact. *Stapp Car Crash Journal* 51: 17-80.
- Ho, J., Zhou, Z., Li, X., and Kleiven, S. (2017) The peculiar properties of the falx and tentorium in brain injury biomechanics. *Journal of Biomechanics* 60: 243-247.
- Horgan, T.J., and Gilchrist, M.D. (2003) The creation of three-dimensional finite element models for simulating head impact biomechanics. *International Journal of Crashworthiness* 8 (4): 353-366.
- Hyder, A.A., Wunderlich, C.A., Puvanachandra, P., Gururaj, G., and Kobusingye, O.C. (2007) The impact of traumatic brain injuries: a global perspective. *NeuroRehabilitation* 22 (5): 341-353.
- Kimpara, H., Nakahira, Y., Iwamoto, M., Miki, K., Ichihara, K., Kawano, S.-i., and Taguchi, T. (2006) Investigation of anteroposterior head-neck responses during severe frontal impacts using a brain-spinal cord complex FE model. *Stapp Car Crash Journal* 50: 509-544.
- Kindberg, K., Karlsson, M., Ingels, N., and Criscione, J. (2007) Nonhomogeneous strain from sparse marker arrays for analysis of transmural myocardial mechanics. *Journal of Biomechanical Engineering* 129 (4): 603-610.
- Kleiven, S. (2007) Predictors for traumatic brain injuries evaluated through accident reconstructions. *Stapp Car Crash Journal* 51: 81-114.
- Kleiven, S., and Hardy, W.N. (2002) Correlation of an FE model of the human head with local brain motion-consequences for injury prediction. *Stapp Car Crash Journal* 46: 123-144.
- Knutsen, A.K., Magrath, E., McEntee, J.E., Xing, F., Prince, J.L., Bayly, P.V., Butman, J.A., and Pham, D.L. (2014) Improved measurement of brain deformation during mild head acceleration using a novel tagged MRI sequence. *Journal of Biomechanics* 47 (14): 3475-3481.

- Kolaczek, S., Hewison, C., Caterine, S., Berardelli, R., Beveridge, T., Herman, B., Hurtig, M., Gordon, K., and Getgood, A. (2019) 3D strain in native medial meniscus is comparable to medial meniscus allograft transplant. *Knee Surgery, Sports Traumatology, Arthroscopy* 27 (2): 349-353.
- Kolaczek, S., Hewison, C., Caterine, S., Ragbar, M., Getgood, A., and Gordon, K. (2016) Analysis of 3D strain in the human medial meniscus. *Journal of the Mechanical Behavior of Biomedical Materials* 63: 470-475.
- Mao, H., Zhang, L., Jiang, B., Genthikatti, V.V., Jin, X., Zhu, F., Makwana, R., Gill, A., Jandir, G., and Singh, A. (2013) Development of a finite element human head model partially validated with thirty five experimental cases. *Journal of Biomechanical Engineering* 135 (11): 111002.
- Margulies, S.S., Thibault, L.E., and Gennarelli, T.A. (1990) Physical model simulations of brain injury in the primate. *Journal of Biomechanics* 23 (8): 823-836.
- Meaney, D.F., Smith, D.H., Shreiber, D.I., Bain, A.C., Miller, R.T., Ross, D.T., and Gennarelli, T.A. (1995) Biomechanical analysis of experimental diffuse axonal injury. *Journal of Neurotrauma* 12 (4): 689-694.
- Morrison, B., Cater, H.L., Wang, C.C., Thomas, F.C., Hung, C.T., Ateshian, G.A., and Sundstrom, L.E. (2003) A tissue level tolerance criterion for living brain developed with an in vitro model of traumatic mechanical loading. *Stapp Car Crash Journal* 47: 93-105.
- Průša, V., Rajagopal, K., and Saravanan, U. (2013) Fidelity of the estimation of the deformation gradient from data deduced from the motion of markers placed on a body that is subject to an inhomogeneous deformation field. *Journal of Biomechanical Engineering* 135 (8): 081004.
- Sabet, A.A., Christoforou, E., Zatlin, B., Genin, G.M., and Bayly, P.V. (2008) Deformation of the human brain induced by mild angular head acceleration. *Journal of Biomechanics* 41 (2): 307-315.
- Takhounts, E.G., Ridella, S.A., Hasija, V., Tannous, R.E., Campbell, J.Q., Malone, D., Danielson, K., Stitzel, J., Rowson, S., and Duma, S. (2008) Investigation of traumatic brain injuries using the next generation of simulated injury monitor (SIMon) finite element head model. *Stapp Car Crash Journal* 52: 1-31.
- Thibault, L.E., Gennarelli, T.A., Margulies, S.S., Marcus, J., and Eppinger, R. (1990) The strain dependent pathophysiological consequences of inertial loading on central nervous system tissue. *Proc. International Conference on the Biomechanics of Impacts*, pp. 191-202.
- Waldman, L.K., Fung, Y., and Covell, J.W. (1985) Transmural myocardial deformation in the canine left ventricle. Normal in vivo three-dimensional finite strains. *Circulation Research* 57 (1): 152-163.
- Van Noort, R., Black, M., Martin, T., and Meanley, S. (1981) A study of the uniaxial mechanical properties of human dura mater preserved in glycerol. *Biomaterials* 2 (1): 41-45.
- Zhang, L., Yang, K.H., and King, A.I. (2001) Comparison of brain responses between frontal and lateral impacts by finite element modeling. *Journal of Neurotrauma* 18 (1): 21-30.
- Zhao, W., Ruan, S., and Ji, S. (2015) Brain pressure responses in translational head impact: a dimensional analysis and a further computational study. *Biomechanics and Modeling in Mechanobiology* 14 (4): 753-766.
- Zhou, Z., Jiang, B., Cao, L., Zhu, F., Mao, H., and Yang, K.H. (2016) Numerical simulations of the 10-year-old head response in drop impacts and compression tests. *Computer Methods and Programs in Biomedicine* 131: 13-25.
- Zhou, Z., Li, X., and Kleiven, S. (2019) Biomechanics of acute subdural hematoma in the elderly: A fluid-structure interaction study. *Journal of Neurotrauma* 36 (13): 2099-2108.
- Zhou, Z., Li, X., and Kleiven, S. (2019) Biomechanics of periventricular injury. *Journal of Neurotrauma* (Under review).
- Zhou, Z., Li, X., and Kleiven, S. (2019) Fluid-structure interaction simulation of the brain-skull interface for acute subdural haematoma prediction. *Biomechanics and Modeling in Mechanobiology* 18 (1): 155-173.
- Zhou, Z., Li, X., Kleiven, S., Shah, C.S., and Hardy, W.N. (2018) A reanalysis of experimental brain strain data: implication for finite element head model validation. *Stapp Car Crash Journal* 62: 293-318.
- Zou, H., Schmiedeler, J.P., and Hardy, W.N. (2007) Separating brain motion into rigid body displacement and deformation under low-

severity impacts. *Journal of Biomechanics* 40 (6): 1183-1191.

APPENDIX A

The Kungliga Tekniska Högskolan (KTH) detailed head model was developed at Royal Institute of Technology in Stockholm by Zhou et al. (2019) using LS-DYNA software. The head model consists of 4.2 million hexahedral elements and 0.5 million quadrilateral elements. The major components in the head are presented in the model, including the skull, the brain, the cerebrospinal fluid (CSF), the ventricle, and the meninges. Material properties of each head component are available in Table A1-A2. It should be clarified that the “average” values for the Ogden-based hyper-viscoelastic constitutive law in Table A2 is used to model the brain.

The head model is validated against experimental data of brain-skull relative motion in Hardy et al. (2007) and tetra-estimated brain strain derived in the current study. For the brain-skull relative motion validation, 6 representative experiments are selected, including one sagittal impact (C288-T3), one horizontal impact (C380-T2), and four coronal impacts (C380-T1, C380-T3, C380-T4, and C380-T6). Strain in cluster 1 (C1) of these 6 selected experiments are further used for strain validation. Details regarding numerical replication of the experimental impacts are available in the “Fidelity evaluation of strain estimation approach” section of the methods of this current study.

Validation results for the brain-skull relative motion are illustrated in Figure A1-A6, while strain validation results are plotted in Figure A7.

Table A2. Ogden hyperelastic and liner viscoelastic constants for the brain material modelling.

	'Soft'	'Average'	'Stiff'
μ_1 (Pa)	26.9	53.8	107.6
μ_2 (Pa)	-60.2	-120.4	-240.8
α_1	10.1	10.1	10.1
α_2	-12.9	-12.9	-12.9
G_1 (MPa)	0.16	0.32	0.64
G_2 (kPa)	39	78	156
G_3 (kPa)	3.1	6.2	12.4
G_4 (kPa)	4.0	8.0	16.0
G_5 (kPa)	0.5	1.0	2.0
G_6 (kPa)	1.5	3.0	6.0
β_1 (1/s)	10^6	10^6	10^6
β_2 (1/s)	10^5	10^5	10^5
⋮	⋮	⋮	⋮
β_6 (1/s)	10^1	10^1	10^1

μ_i and α_i are Ogden parameters, G_i represents the shear relaxation moduli, β_i are the decay constants.

Table A1. Material properties for the FE head model.

Tissue	Young's modulus (MPa)	Density (kg/dm ³)	Poisson's ratio	Reference
Cortical bone	15000	2.00	0.22	(Kleiven, 2007)
Porous bone	1000	1.3	0.24	(Kleiven, 2007)
Brain	Hyper-Viscoelastic	1.04	~0.5	(Kleiven, 2007)
CSF/Ventricle	K = 2.1 GPa	1.00	--	(Kleiven, 2007)
Dura/Falx/Tentorium	Average stress-strain curve	1.13	--	(Aimedieu and Grebe, 2004)
Pia	Average stress-strain curve	1.13	--	(Van Noort et al., 1981)

K: Bulk modulus

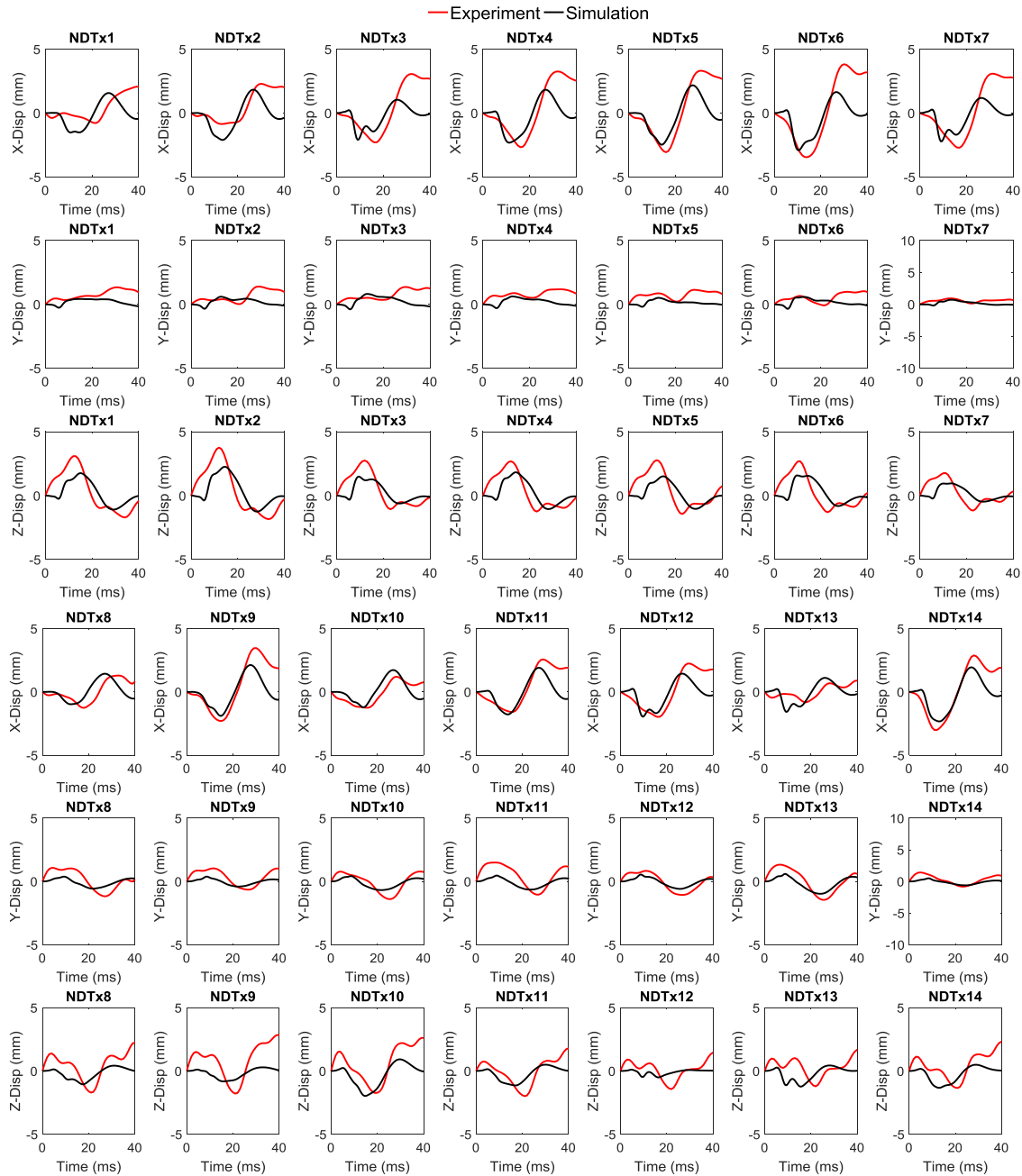


Figure A1. Comparison between experimental motion and simulated brain-skull relative motion for the experiment C288-T3.

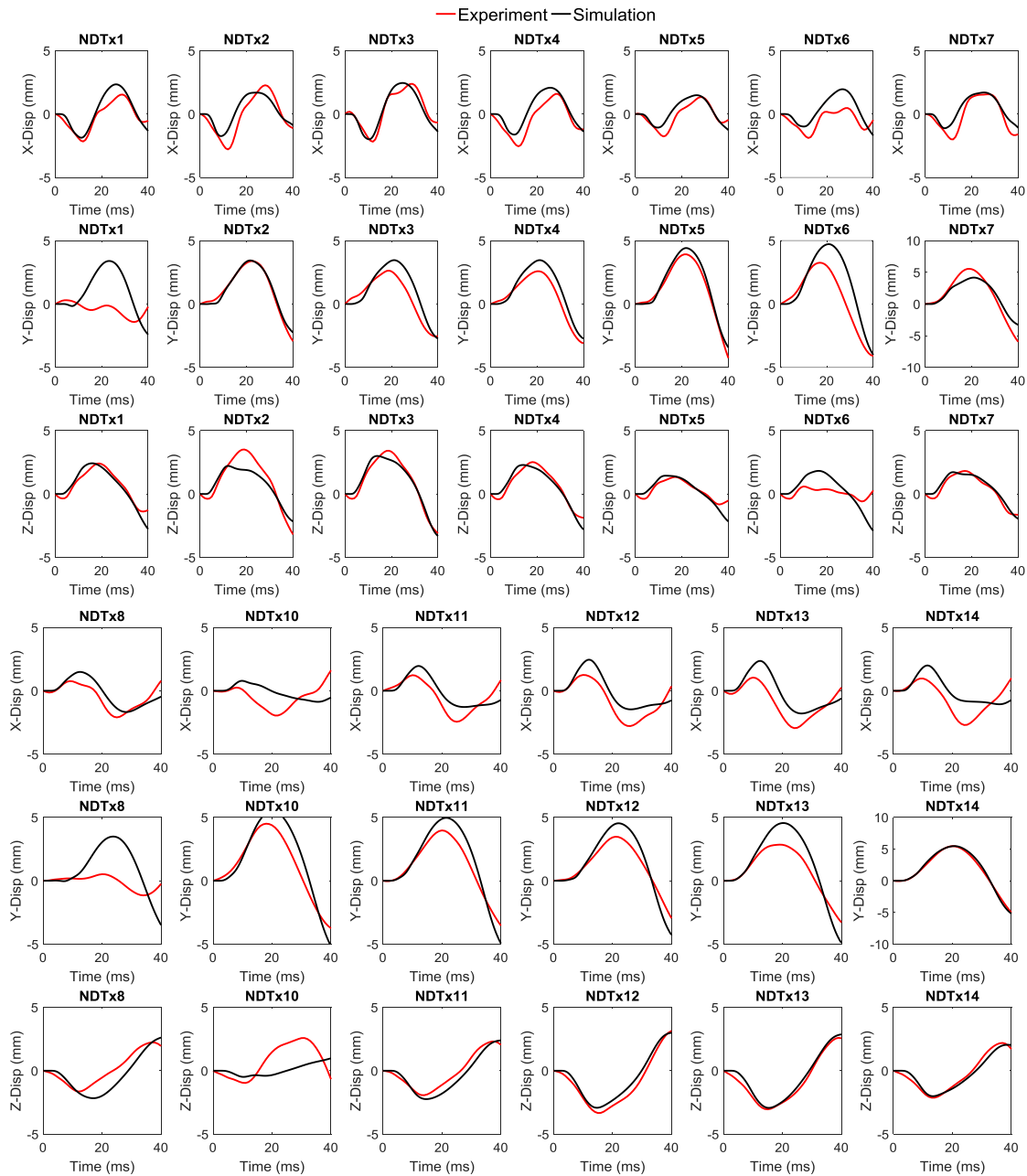


Figure A2. Comparison between experimental motion and simulated brain-skull relative motion for the experiment C380-T1.

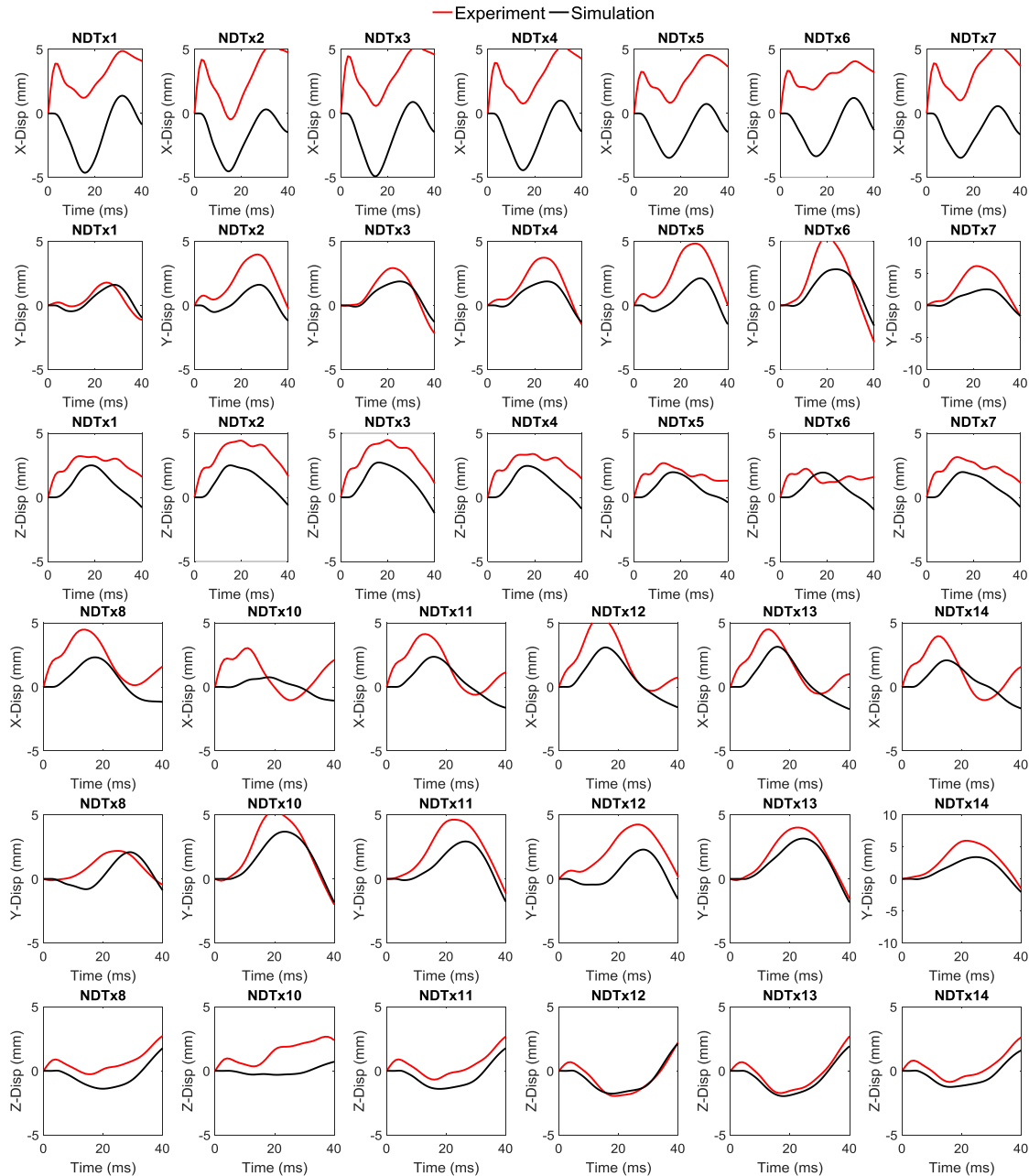


Figure A3. Comparison between experimental motion and simulated brain-skull relative motion for the experiment C380-T2.

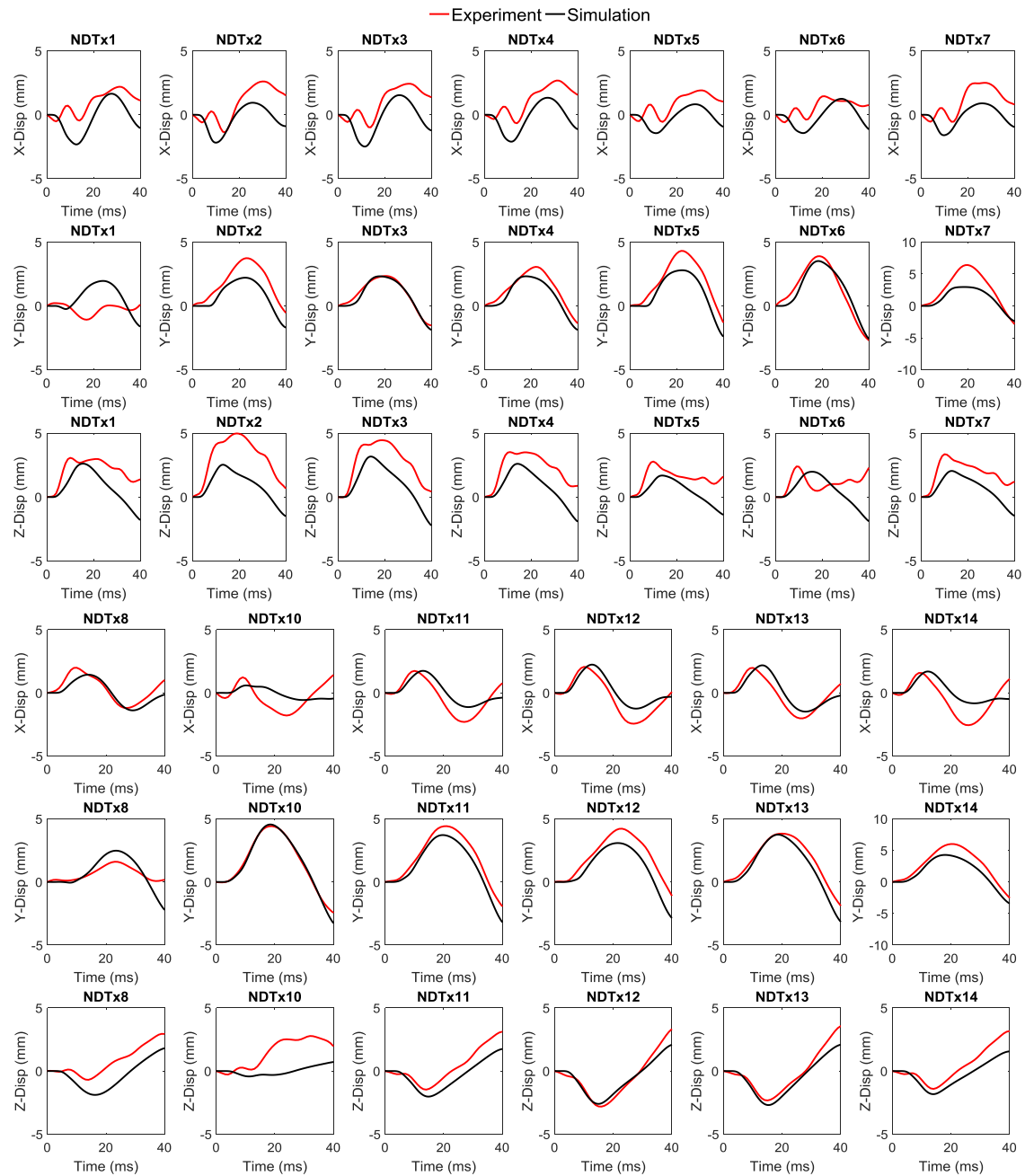


Figure A4. Comparison between experimental motion and simulated brain-skull relative motion for the experiment C380-T3.

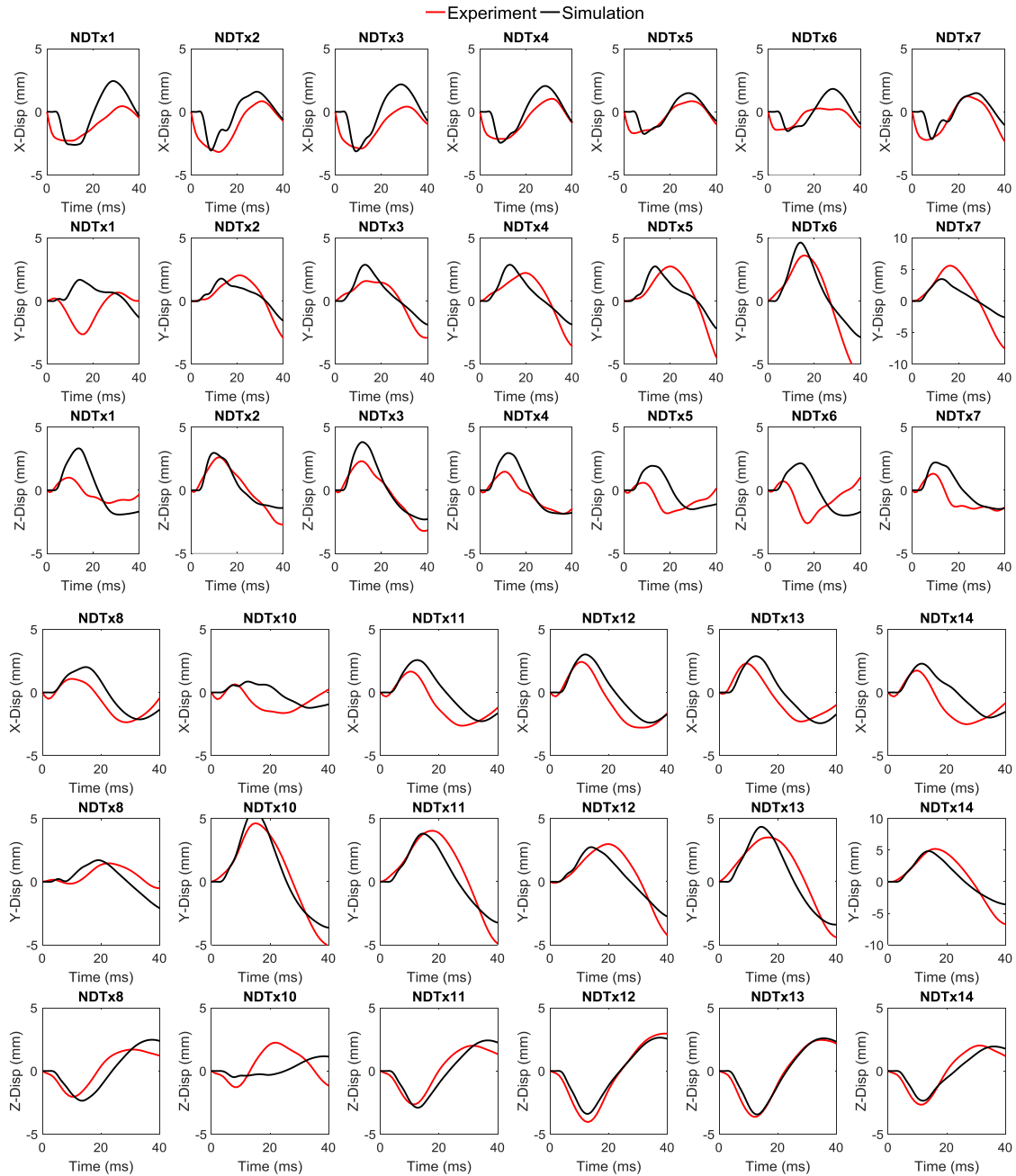


Figure A5. Comparison between experimental motion and simulated brain-skull relative motion for the experiment C380-T4.

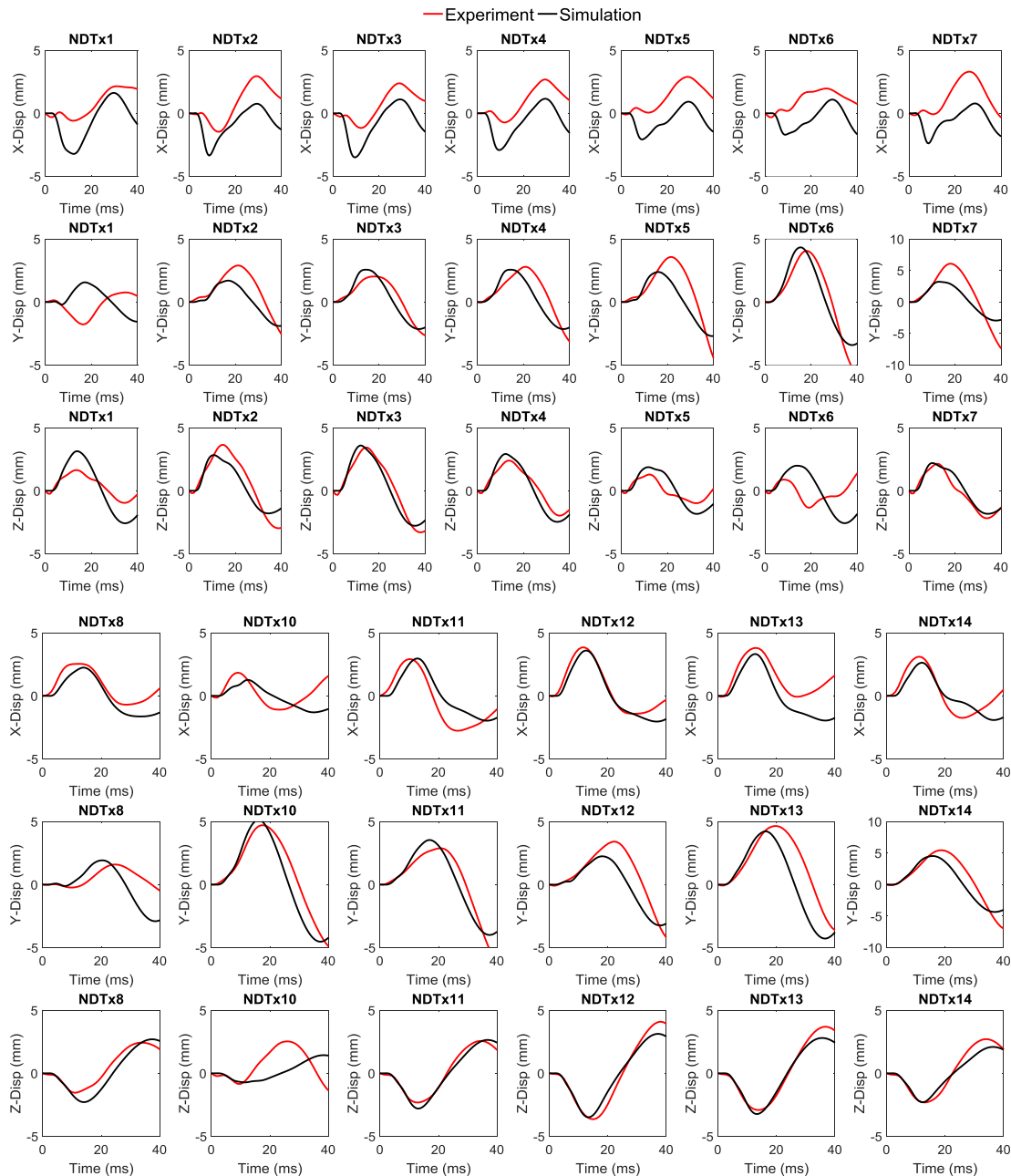
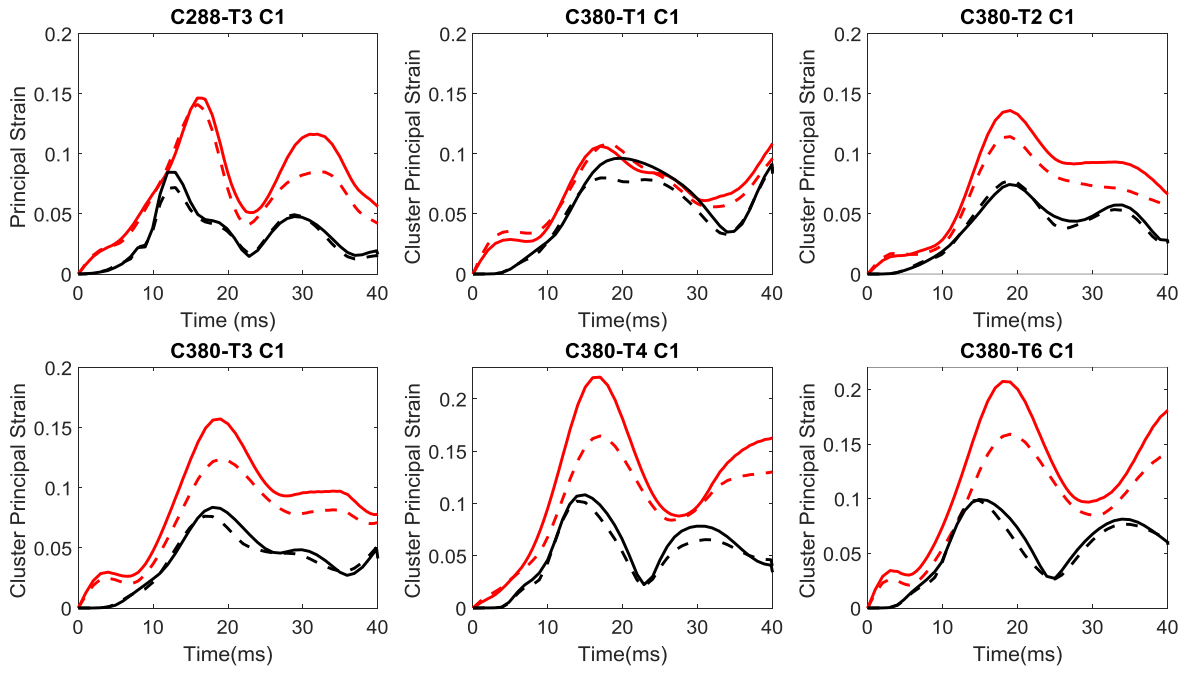


Figure A6. Comparison between experimental motion and simulated brain-skull relative motion for the experiment C380-T6.



— Experimental Principal Strain — Experimental Shear Strain — Numerical Principal Strain - - Numerical Shear Strain
 Figure A7. Comparison between experimental tetra strain and numerical strain estimated by the tetra approach.

APPENDIX B

For the cluster 2 (C2) for five impacts delivered to C380, only one NDT, i.e. NDT 9, was not reliably tracked. Thus, an additional model is developed with

4 tetrahedron elements (Figure B1 (a)) is developed to estimate the strain with the results in Figure B1 (b).

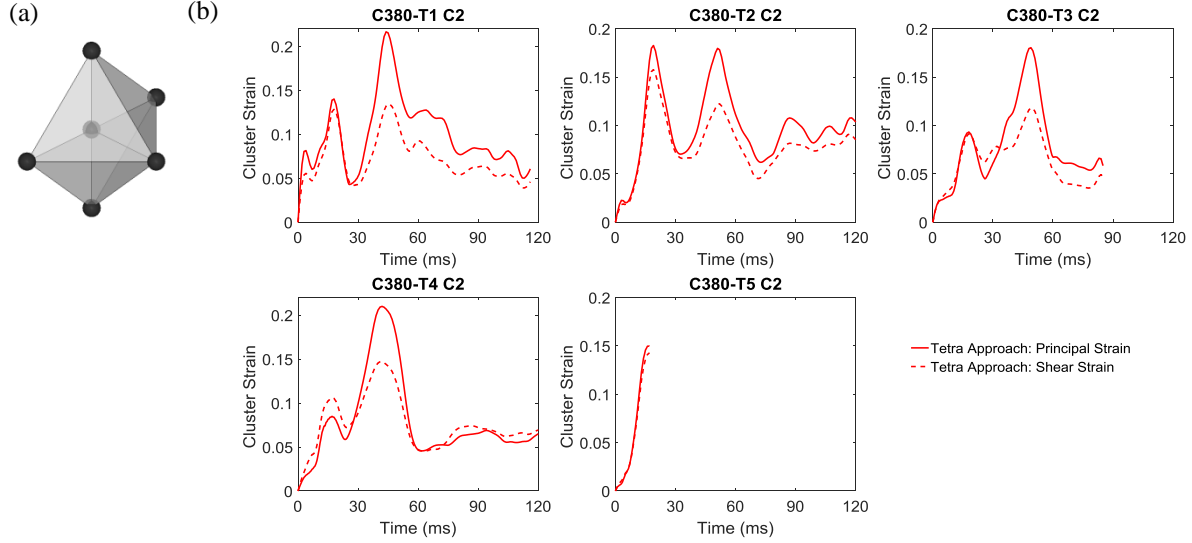


Figure B1. (a) Strain estimation by the tetra approach for C2 in C380 that 6 NDT were reliably tracked. The NDTs are shown as black spheres, while tetrahedron elements in grey and mesh line in black. To visualize the center NDT, all tetrahedron elements are shown in translucency. (b) Strain responses of C2 in C380 estimated by the tetra approach.

APPENDIX C

To test the dependency of the evaluation results regarding the fidelity of strain estimation approach on brain material stiffness, an Ogden-based hyper-viscoelastic constitutive law with material constant sets referred to as “soft” and “stiff” in Table A2 is alternatively adopted to describe the brain material in the Kungliga Tekniska Högskolan (KTH) detailed head model. Material constants for the “soft” set are equivalent to half of these “average” set, while the long-term shear modulus with constants of the “stiff” set is twice as that of the “average” set, similar to the approach used by Kleiven (2007) and Zhao et al. (2015).

To test the dependency of the evaluation results regarding the fidelity of strain estimation approach on the constitutive law for brain, a viscoelastic material is alternatively used to describe the brain material in the KTH detailed head model, as similarly used in previously published head models (Horgan and Gilchrist, 2003, Kimpara et al., 2006, Takhounts et al., 2008, Zhang et al., 2001, Zhou et al., 2016). As listed in Table C1, material constants for the gray matter in the Global Human Body Models Consortium (GHBMC) head model (Mao et al., 2013) are adopted.

To test the model dependency of the evaluation results regarding the fidelity of strain estimation approach, two independently-developed head models, i.e. the Total Human Model for Safety (THUMS) head model (Kimpara et al., 2006) and the GHBMC head model (Mao et al., 2013), are alternatively selected.

These five models are used to simulate one representative experimental impact (C380-T4) as well as the associated strain estimation procedures. Details regarding numerical replication of the experimental impacts are available in the “Fidelity evaluation of strain estimation approach” section of the methods of this current study.

Influence of brain stiffness and the brain constitutive law on brain-skull relative motion validation and brain strain validation for the KTH detailed head model, and validation results for the THUMS head model and the GHBMC head model are illustrated in Figure C1-C6.

Influence of brain stiffness, the constitutive law used for the brain, and head model choice on the evaluation results regarding the fidelity of strain estimation approach is illustrated in Figure 7.

Table C1. Viscoelastic material properties for the brain.

Tissue	Bulk modulus (GPa)	Density (kg/dm ³)	Short-time shear modulus (kPa)	Long-time shear modulus (kPa)	Decay constant	Reference
Brain	2.19	1.04	6.0	1.2	80	(Mao et al., 2013)

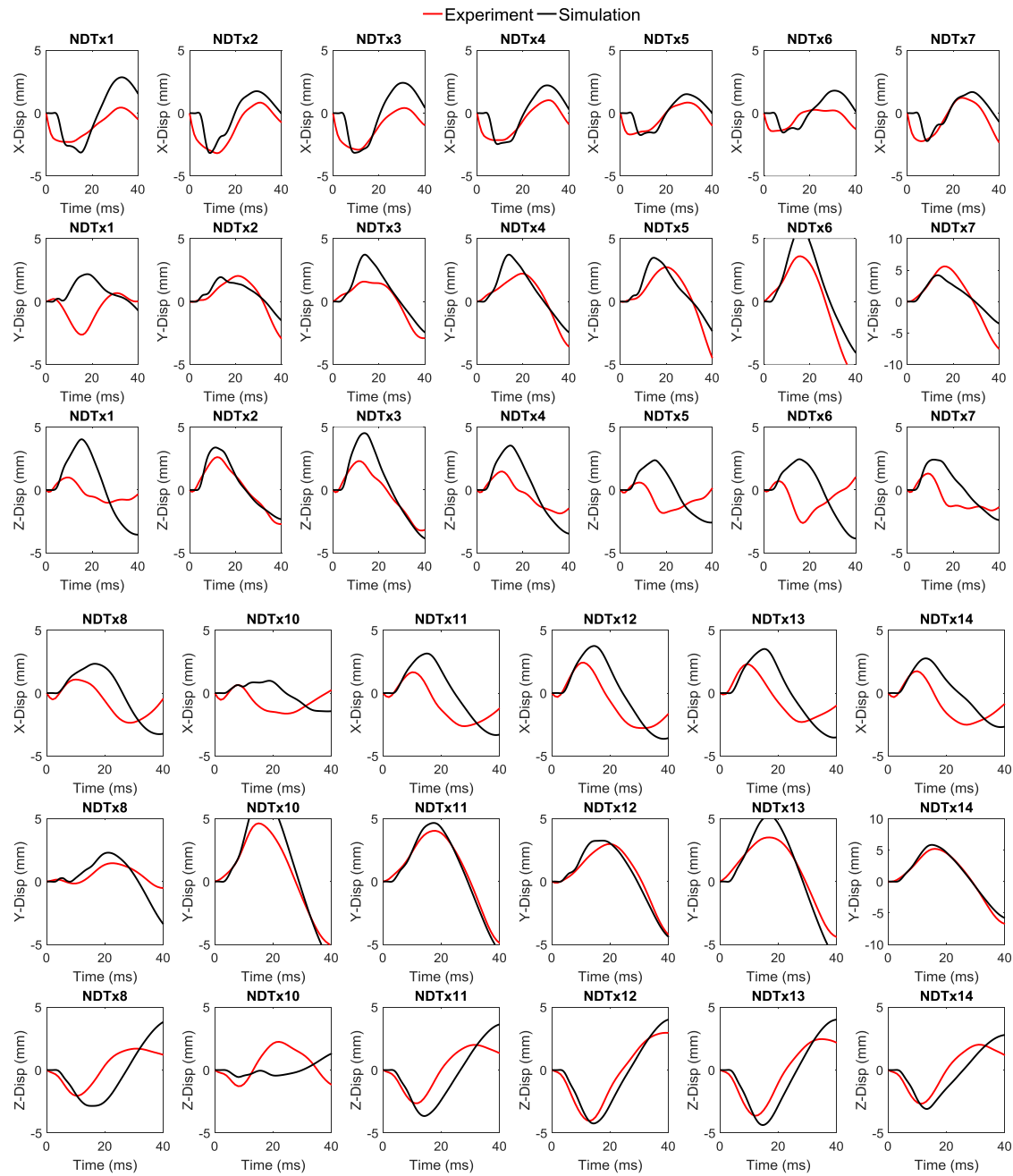


Figure C1. Comparison between experimental motion and brain-skull relative motion predicted by the KTH detailed head model with the brain represented by an Ogden-based material with “soft” constants for the experiment C380-T4.

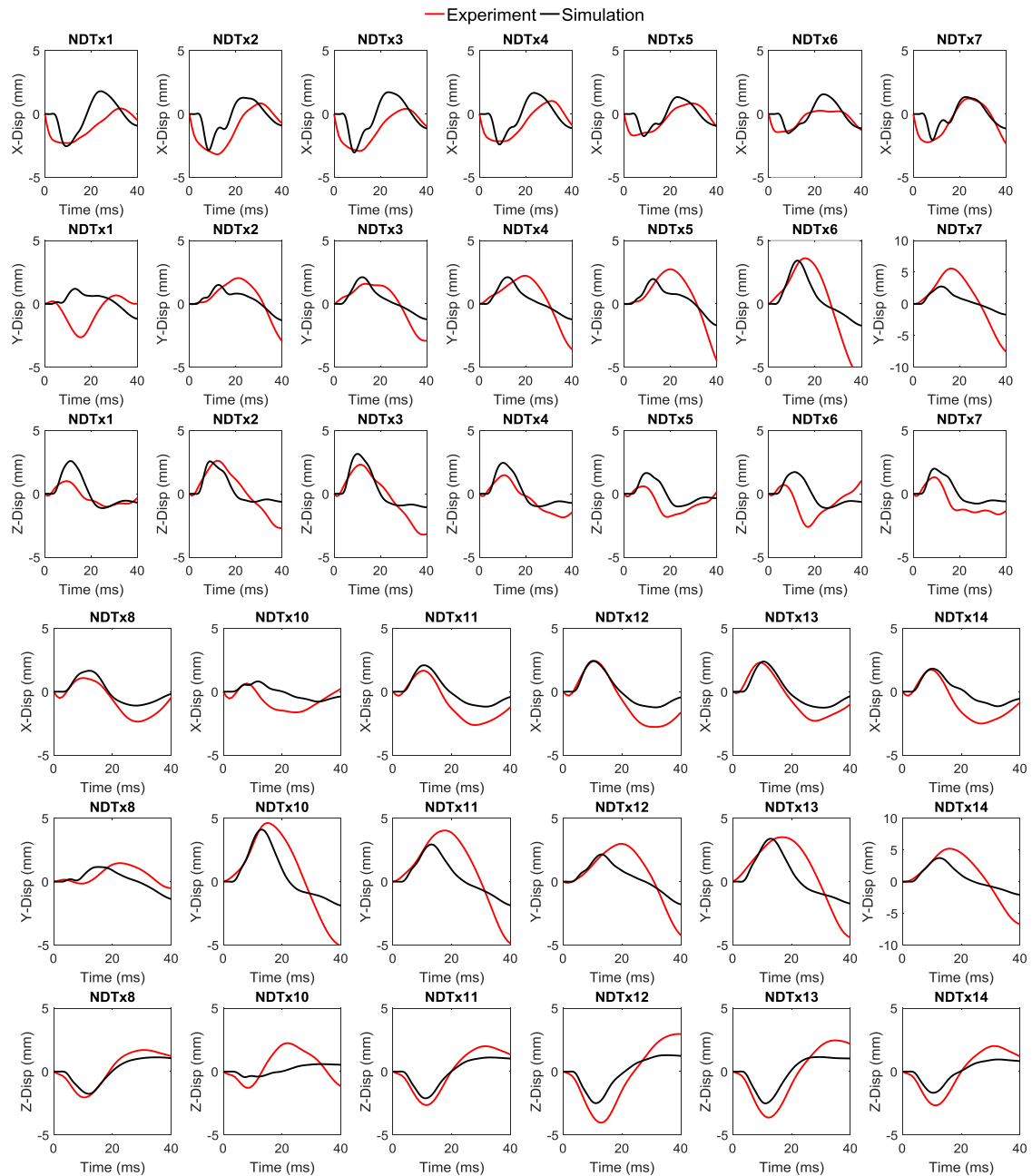


Figure C2. Comparison between experimental motion and brain-skull relative motion predicted by the KTH detailed head model with the brain represented by an Ogden-based material with “stiff” constants for the experiment C380-T4.

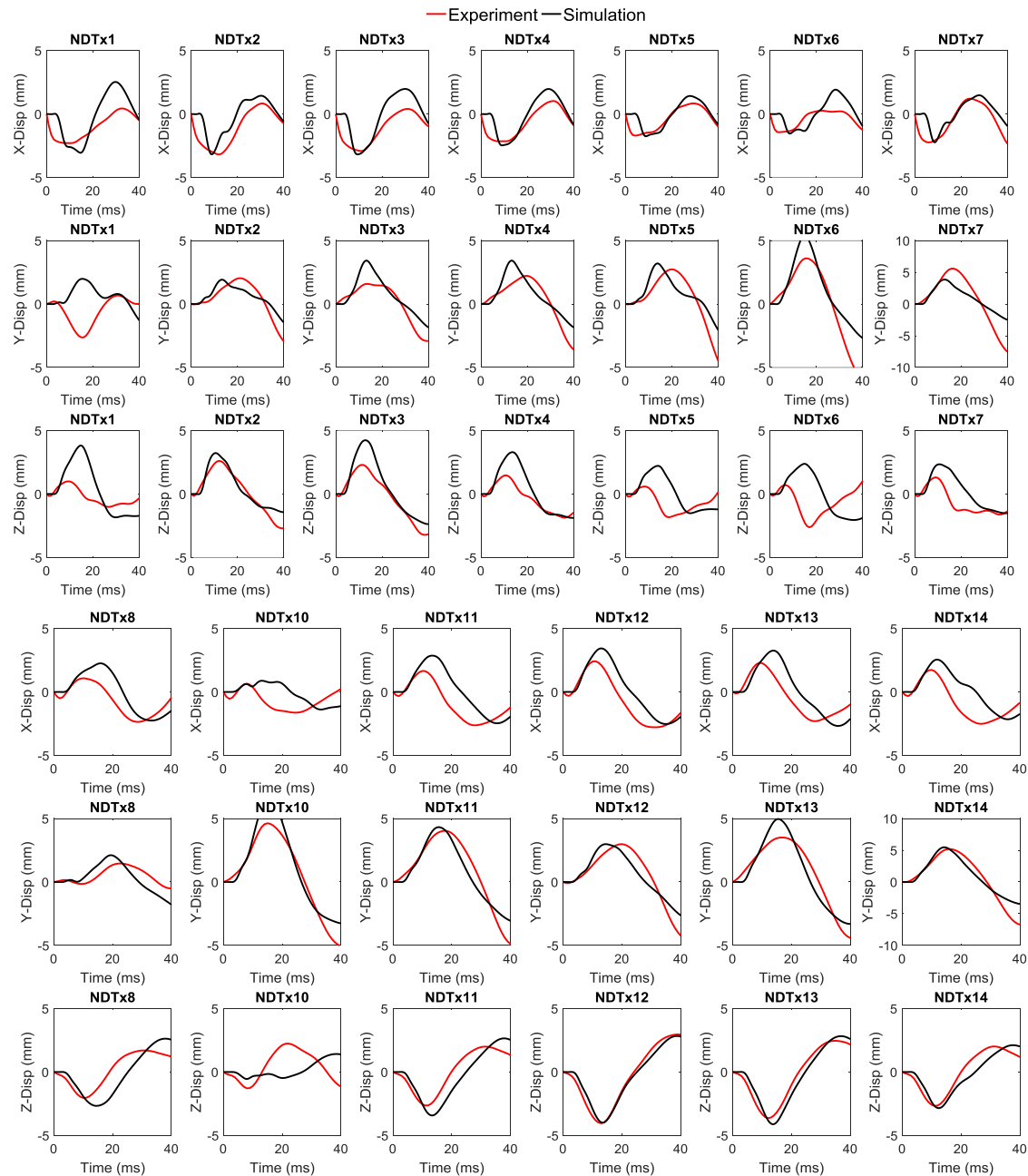


Figure C3. Comparison between experimental motion and brain-skull relative motion predicted by the KTH detailed head model with the brain represented by a viscoelastic material for the experiment C380-T4.

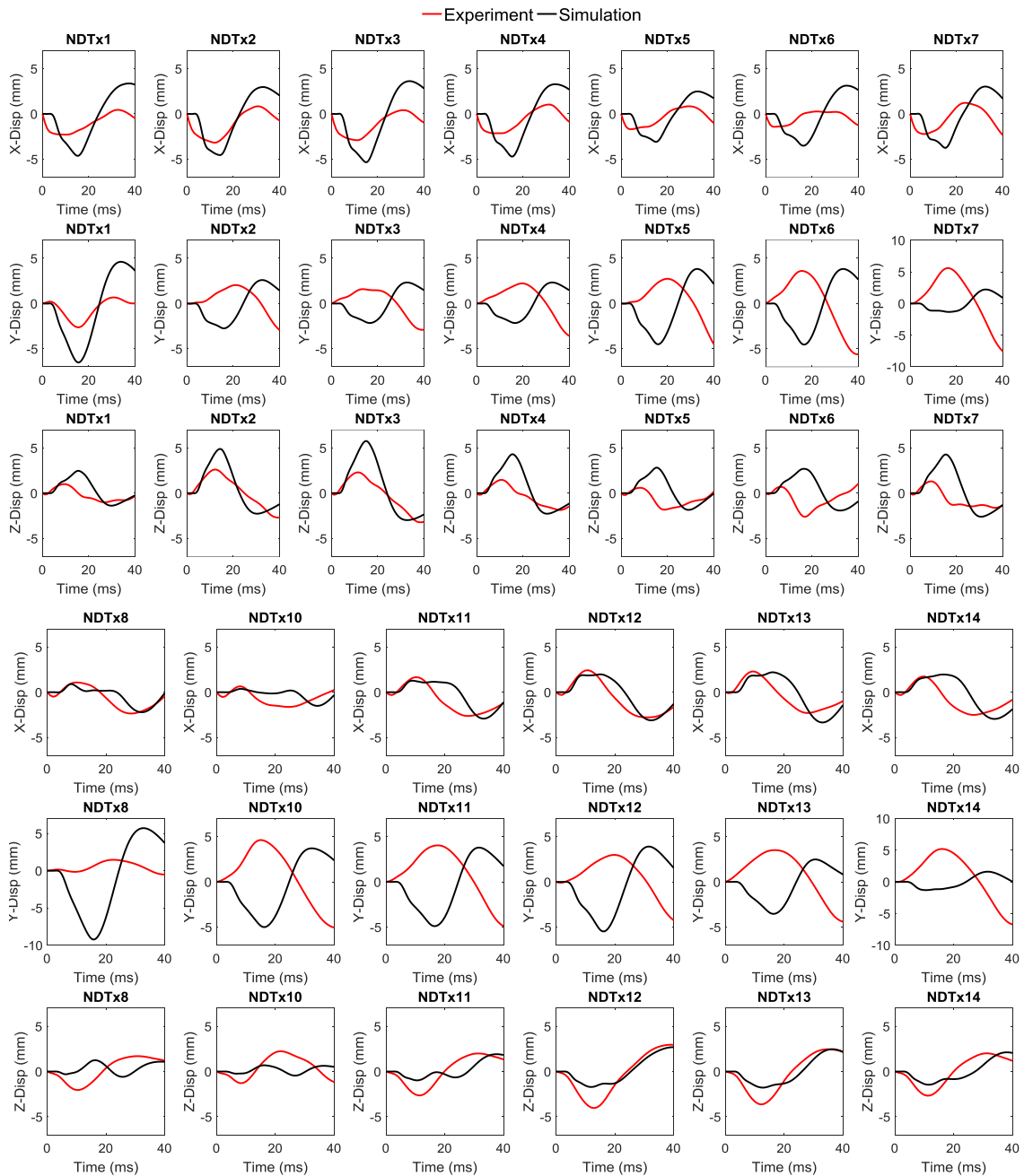


Figure C4. Comparison between experimental motion and brain-skull relative motion predicted by the THUMS head model for the experiment C380-T4.

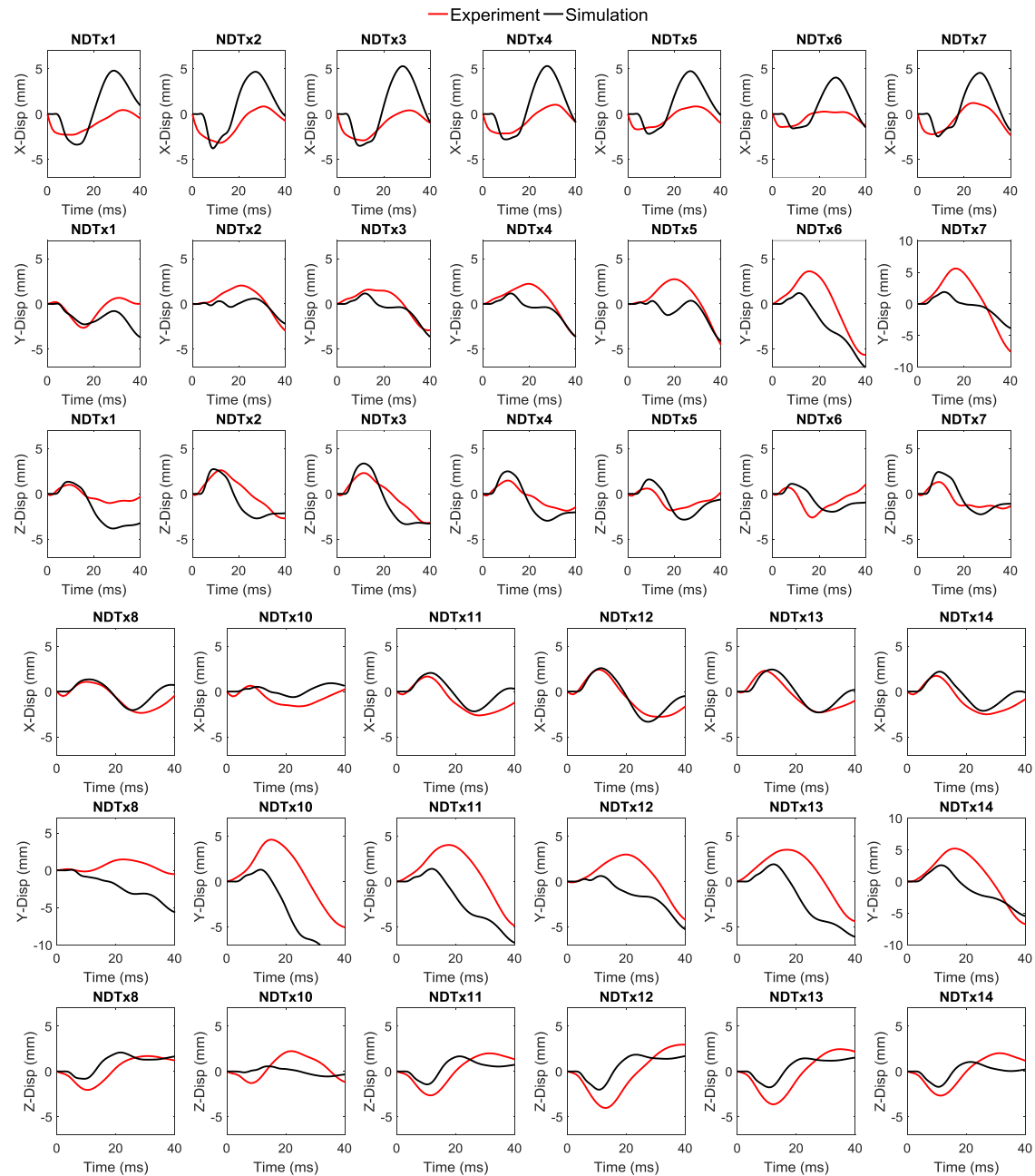


Figure C5. Comparison between experimental motion and brain-skull relative motion predicted by the GHBMC head model for the experiment C380-T4.

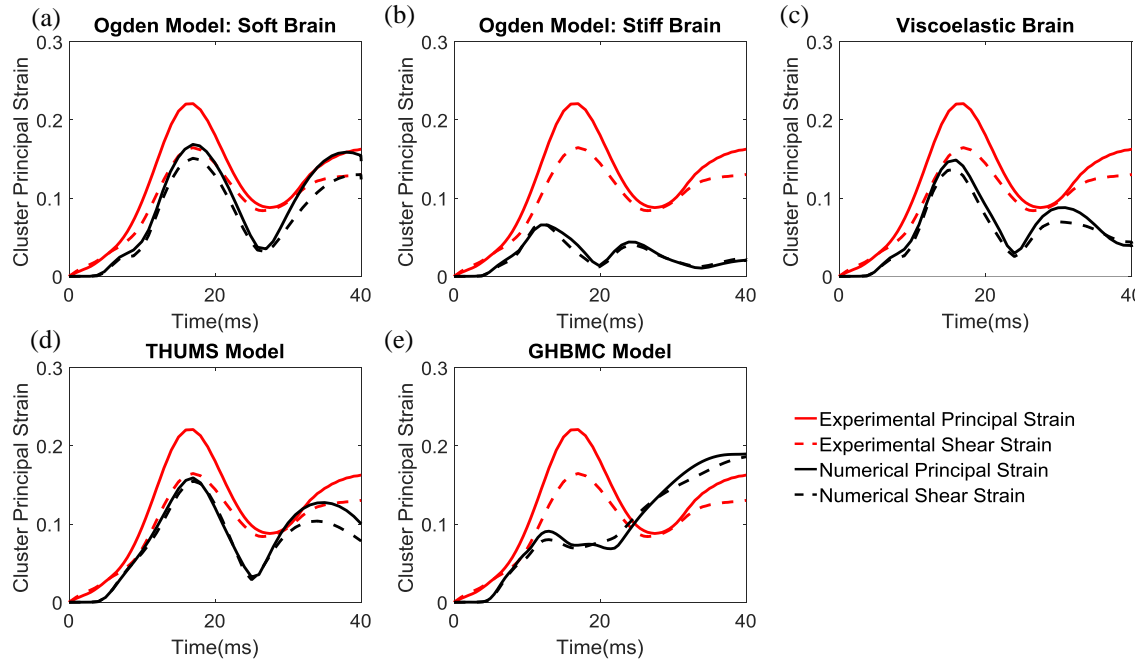


Figure C6. Influence of the brain stiffness and brain constitutive law for the strain validation of the KTH detailed head model and strain validation results of the THUMS head model for the experiment C380-T4. (a) Strain validation of the KTH detailed head model with the brain represented by an Ogden-based material with “soft” constants. (b) Strain validation of the KTH detailed head model with the brain represented by an Ogden-based material with “stiff” constants. (c) Strain validation of the KTH detailed head model with the brain represented by a viscoelastic material. (d) Strain validation of the THUMS head model. (e) Strain validation of the GHBMC head model.

Reproduced with permission of copyright owner. Further reproduction
prohibited without permission.